Physics of Beer Tapping

Javier Rodríguez-Rodríguez,[1,*] Almudena Casado-Chacón,[1] and Daniel Fuster[2]
[1]Fluid Mechanics Group, Carlos III University of Madrid, 28911 Leganés, Madrid, Spain
[2]CNRS (UMR 7190), Université Pierre et Marie Curie. Institute Jean le Rond D'Alembert, 75005 Paris, France
(Received 27 April 2014; revised manuscript received 15 September 2014; published 20 November 2014)

The popular bar prank known in colloquial English as beer tapping consists in hitting the top of a beer bottle with a solid object, usually another bottle, to trigger the foaming over of the former within a few seconds. Despite the trick being known for a long time, to the best of our knowledge, the phenomenon still lacks scientific explanation. Although it seems natural to think that shock-induced cavitation enhances the diffusion of CO_2 from the supersaturated bulk liquid into the bubbles by breaking them up, the subtle mechanism by which this happens remains unknown. Here, we show that the overall foaming-over process can be divided into three stages where different physical phenomena take place in different time scales: namely, the bubble-collapse (or cavitation) stage, the diffusion-driven stage, and the buoyancy-driven stage. In the bubble-collapse stage, the impact generates a train of expansion-compression waves in the liquid that leads to the fragmentation of preexisting gas cavities. Upon bubble fragmentation, the sudden increase of the interface-area-to-volume ratio enhances mass transfer significantly, which makes the bubble volume grow by a large factor until CO_2 is locally depleted. At that point buoyancy takes over, making the bubble clouds rise and eventually form buoyant vortex rings whose volume grows fast due to the feedback between the buoyancy-induced rising speed and the advection-enhanced CO_2 transport from the bulk liquid to the bubble. The physics behind this explosive process sheds insight into the dynamics of geological phenomena such as limnic eruptions.

DOI: 10.1103/PhysRevLett.113.214501 PACS numbers: 47.55.P-, 47.55.dp

Understanding the formation of foam in a supersaturated carbonated liquid after an impact on the container involves a careful physical description of a number of processes of great interest in several areas of physics and chemistry. The following happens in order of appearance in this problem: propagation of strong pressure waves in bubbly liquids, bubble collapse and fragmentation, gas-liquid diffusive mass transfer, and the dynamics of bubble-laden plumes and vortex rings. All these phenomena are observed, for instance, in the explosive formation of foam occurring in a beer bottle when it is tapped on its mouth, an effect known as beer tapping. In this Letter, we will use this effect as a convenient system to quantitatively describe the interaction between the processes mentioned above that ultimately leads to the explosive formation of foam that occurs in gas-driven eruptions [1]. As a consequence of the broad range of phenomena taking part in the overall process, the better understanding of the foam forming process in supersaturated liquids finds application in various fields of natural sciences and technology where similar gas-driven eruptions occur. The dynamics of limnic [1,2] or explosive volcanic [3,4] eruptions and the formation of flavor-releasing aerosols by bursting Champagne bubbles [5] are just a few examples. Mott and Woods [6] have triggered a chain reaction in a stably stratified tank containing a deep layer of CO_2-saturated lemonade and a shallower layer of fresh water by spilling a gravity current of salt grains along the bottom of the tank. This example shows that the dynamics of CO_2 bubbles in daily life liquids can be used to explain complex natural phenomena such as limnic eruptions.

To understand how the processes described above interact to lead to the foaming up of beer, we have carried out an experimental investigation impacting commercial beer bottles under well-controlled repeatable conditions (see Supplemental Material [7]). In particular, bubbles have been generated at a fixed location far from the bottle walls by focusing a laser pulse into the bulk liquid. In this way, we avoid the variability in the formation of bubbles upon the impact caused by the arbitrary distribution of nucleation sites [8], thus, ensuring that a bubble with a known initial size is always present in the measurement volume. By recording the evolution of these gas bubbles with a high-speed camera and the liquid pressure temporal evolution with a hydrophone, we provide qualitative and quantitative analyses of the various processes that develop during the foam formation. We divide the overall foaming-over process into well-differentiated stages controlled by different physical mechanisms and, more importantly, we show experimental evidence supporting the explanation given for each step of the outgassing process.

The chain of events that ultimately leads to the foaming up of beer is triggered by a sudden impact on the top of the bottle, which generates a compression wave that propagates through the glass towards the bottom as predicted by the classical theory of impact on solids [9]. When the wave reaches the base of the bottle, it is partially transmitted to

the liquid as an expansion wave that travels towards the free surface, where it bounces back as a compression wave. A simple model for the impact problem [9] predicts that the stiffer the bottle, the more efficient is the transmission of the expansion wave to the liquid. Thus, the shock is more efficiently transmitted into the liquid in the case of a glass container than in a softer bottle (e.g., plastic). Although, in this case, the expansion wave would still be generated, its amplitude would be smaller. The train of waves transmitted to the liquid bounce back and forth several times until it damps out. Figure 1 shows snapshots of the first instants after the impact to illustrate the effects of the first expansion-compression cycle. It can be seen how bubbles start to expand first near the bottom, whereas, at approximately $t \approx 124$ μs, those located near the free surface begin to shrink. The train of rarefaction-compression waves drives the fragmentation of most of the existing gas pockets during the first wave cycles. Figure 2 illustrates a typical time evolution of the bubble radius measured in our experiments along with snapshots showing the bubble at different relevant instants of the expansion-collapse process (see also Movies S1 and S2 in the Supplemental Material [7]). This first stage of the overall foaming-up process lasts of the order of the acoustic time of the liquid volume, usually $t_{ac} = 2H/c \approx 0.2$ ms, assuming a typical liquid height $H \approx 10$ cm and a speed of sound around $c \approx 1000$ m/s. Notice that, since waves propagating in bubbly liquids are strongly damped, the intensity of successive rebounded waves decays rapidly, thus, they are less likely to cause bubble collapse.

Similar to what happens in the generation of medical ultrasound contrast agents through sonication (Ref. [10]) or, albeit in a more violent way, in sonoluminescence [11], it seems reasonable to attribute the breakup of the bubbles to a Rayleigh-Taylor instability [11]. The number of fragments, N, resulting upon the break up of a bubble cannot be measured due to the high void fraction of the resulting bubble cloud [Fig. 2(d)]. Instead, an estimation of this number is obtained using the model of Brennen [12],

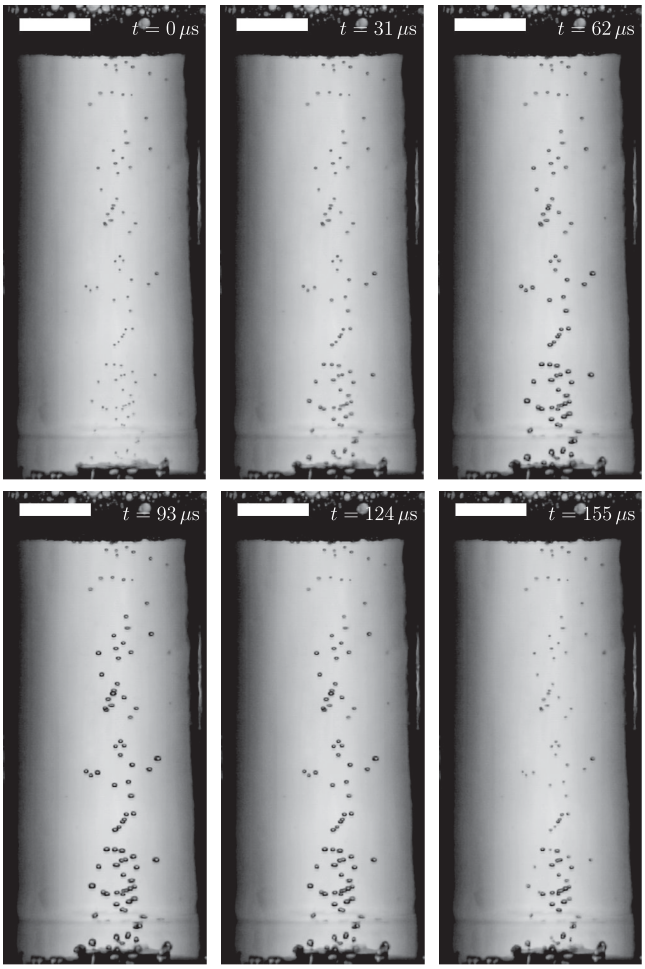

FIG. 1. Sequence of images corresponding to the instants right after the pressure wave starts to propagate through the beer. To ensure a continuous bubble cloud, a metal disk was placed at the bottom of the bottle in this experiment, what effectively introduces a large number of nucleation sites. Scale bar: 10 mm.

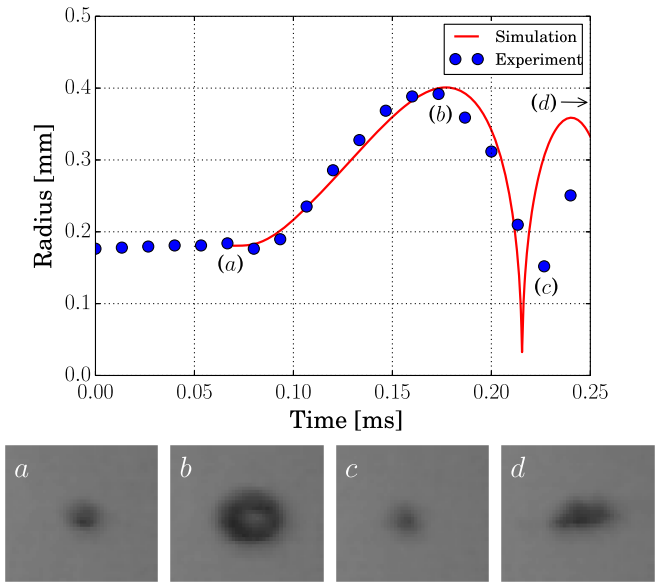

FIG. 2 (color online). A bubble of initial radius $R_0 \approx 180$ μm, induced by a laser pulse nearly a second before the impact, grows after the passage of the expansion wave reaching the bubble location at instant (a). After the instant of maximum radius (b), the bubble collapses at some point between frame (c) and the previous one, turning into a bubble cloud. Panel (d) shows the bubble cloud 0.1 ms after instant (c). The Rayleigh-Plesset equation has been integrated numerically (red solid line, see Supplemental Material [7]) for a bubble subjected to a pressure pulse with an amplitude, $p_A = 100$ kPa, and period, $T = 0.24$ ms, measured at the bubble's location with a hydrophone. Notice that, after the implosion, $t \approx 0.22$ ms, the Rayleigh-Plesset equation no longer describes the behavior of the bubble since it is only valid for a single bubble, not for a bubble cloud. (see Movies S1 and S2).

based on the ideas put forward by several authors [13,14]. Following this model (see Supplemental Material [7]), the most unstable mode is given by

$$n_m = \frac{1}{3}((7 + 3\Gamma_m)^{1/2} - 2), \tag{1}$$

with $\Gamma_m = \rho R^2 \ddot{R}/\sigma$, evaluated at the instant when the radius, R, is minimum, ρ the fluid density, and σ the liquid-gas surface tension. The size of the fragments is expected to be of the order of R/n_m; thus, the number of fragments generated is $N \approx n_m^3$. For the typical bubble sizes and pressure wave amplitudes used in these experiments, we find a most unstable mode of the order of $n_m \approx 10^2$ and a number of fragments $N \approx 10^6$.

As a consequence of the fast bubble collapse and breakup, right after the implosion, the total gas-liquid interfacial area increases by a factor of the order of $N^{1/3}$. This sudden increase of the interfacial area leads to a second stage where the clouds of bubble fragments grow rapidly as a result of the diffusion of carbonic gas into the newly created cavities. This stage can be modeled using the classical theory of bubble growth in supersaturated media (Ref. [15]). Under the reasonable assumption that the cloud grows as the sum of its components, this theory states that the cloud size, L_c, follows

$$L_c = L_0 + \alpha N^{1/3} F\left(\frac{\Delta C}{\rho_g}\right)\sqrt{\frac{\kappa t}{\pi}}, \tag{2}$$

where ΔC is the difference between the concentration of carbonic gas in the bulk liquid and the saturation value, κ its diffusivity, ρ_g the density of the gas inside the bubbles, α a dimensionless constant, and $F(x)$ a known function (see Supplemental Material [7]). Taking the estimated number of fragments generated during the collapse of a single bubble, $N \approx 10^6$, we expect the radius of the bubble cloud to grow about 100 times faster than a single bubble with the same volume than the cloud. In fact, this magnitude represents an upper bound, since those fragments at the center of the cloud will grow more slowly, due to their limited access to CO_2. Initially, the growth rate scales roughly as $t^{1/2}$ albeit exhibiting some oscillations caused by cycles of expansions and compressions that are not yet attenuated (see the stage labeled "diffusion-driven" in Fig. 3, blue circles in the upper panel). This diffusion-driven stage ends when carbon dioxide is locally depleted, and thus, the cloud's size significantly moderates its growth.

In the example of Fig. 3, this occurs at about $t \approx 10$ ms (stage labeled as "depletion"). To avoid the noise introduced by the acoustic waves at short times, we have performed additional experiments by focusing a high-energy laser pulse inside the liquid to trigger the formation of a bubble cloud by laser-induced cavitation [16]

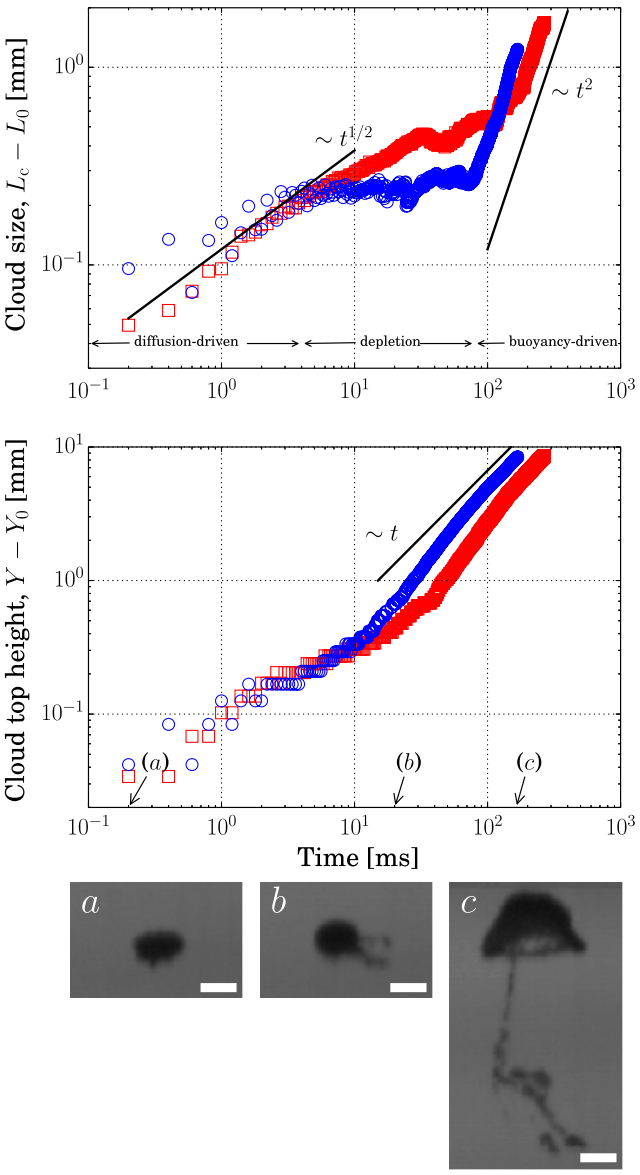

FIG. 3 (color online). Upper plot: Time evolution of the size of a bubble cloud, L_c, after the shock-induced collapse of an already existing bubble (blue circles) and after a laser-induced bubble implosion (red squares). Three different stages have been marked qualitatively: diffusion driven, depletion, and buoyancy driven. Black solid lines depict the scaling laws $L_c \sim t^{1/2}$ (diffusion driven) and $L_c \sim t^2$ (buoyancy driven). Lower plot: Time evolution of the top of the bubble cloud corresponding to the same cases of the upper plot. Notice how, at long times, the plume approaches a steady rising velocity. Letters denote the instants corresponding to the images in the lower panels (scale bar: 1 mm). (See Movie S3 in the Supplemental Material [7]).

(see Supplemental Material [7]). In the focal region, the laser generates a dense bubble cloud that initially grows as the square root of time, which is consistent with a purely diffusive growth (Fig. 3, red squares in the upper panel).

The rapidly growing bubble clusters act as buoyancy sources that lead to the formation of bubble-laden buoyant

vortex rings in time scales of order $t_g \sim (L/g)^{1/2}$ [Fig. 3(c)], very much like a localized release of heat forms a thermal [17]. As the vortices rise through the liquid, the advection due to their self-induced velocity and the mixing caused by their vortical motion contribute to enhance the transport of CO_2 to the bubbles. In turn, this results in a growth rate faster than that found for pure diffusion, namely $t^{1/2}$. Indeed, the cloud's size grows roughly as t^2 during this stage (Fig. 3, upper plot).

As a consequence of the continuous generation of gas volume inside the vortex, the velocity approaches a constant value (Fig. 3, lower plot) instead of decreasing as happens in buoyant vortex rings induced by the release of a fixed amount of buoyancy. For instance, in thermals originated by the sudden release of a fixed amount of heat, the velocity decays as $t^{-1/2}$ due to the entrainment of colder fluid [17,18]. Conversely, in the bubble-laden plumes studied here, the feedback between buoyancy-driven rising motion and gas-volume generation results in a nearly constant speed. This behavior is similar to that found in the the so-called autocatalytic vortex rings or plumes [19] where buoyancy is continuously produced by a chemical reaction that yields products less dense than the reactants. These buoyancy-driven chemically reacting flows appear, for instance, in the combustion of flame balls in microgravity conditions. Interestingly, they are also relevant in some explosion scenarios for type Ia supernovae [20,21].

The analogy between the bubble-laden plumes observed here and the autocatalytic plumes described in the literature also extends to their morphology. Panel (c) in Fig. 3 shows one of these bubble-laden plumes when it is well developed (see also Movie S3 in the Supplemental Material [7]). The plume consists of a vortex with a nearly spherical cap with a thin conduit that ascends more slowly, features observed in the plumes driven by autocatalytic chemical reactions [19,21].

It should be pointed out that, among all the stages of the foaming-up process, this one is the most effective in terms of the amount of liquid outgassing as a result of its self-accelerating nature. This stage starts at times of the order of tens of milliseconds and concludes when the plumes reach the size of the liquid volume, usually of the order of a second.

Remarkably, the behavior of the bubble-laden vortex rings during the diffusion-driven and buoyancy-driven stages is independent of the mechanism used to generate the initial bubble cloud. Figure 3 depicts the evolution of the bubble cluster size and velocity of a bubble cluster originated by laser-induced cavitation. The size and velocity follow the same scaling laws as the vortex created by the pressure-induced bubble implosion. This suggests that similar explosive CO_2 outgassing processes driven by the formation of these bubbly plumes may be initiated by other physical mechanisms generating dense bubble clouds such as the introduction of new bubble nucleation sites [22,23] or a sudden change of the saturation conditions occurring either globally [4] or locally [2,23]. In fact, our observations suggest that, once the plume is initiated, its dynamics does not seem to depend on the particular initiation mechanism. Thus, one of the main conclusions of this study is that the dynamics of these bubble-laden self-accelerating plumes moving in supersaturated media may partly explain the explosive behavior of systems such as limnic and explosive volcanic eruptions where current models typically neglect the role of these autocatalytic structures [1,3,4,6,23].

Finally, two side effects induced by the development of the bubbly plumes must be mentioned here attending to their relevance in the global degassing process in the case of the bottle. First, due to the finite size of the container, a global recirculating motion is generated that drags bubbles from near the free surface deep into the bulk liquid, thus, increasing their residence time in the flow and allowing them to grow for longer times. Second, the flow induced inside the bottle also speeds up the growth of gas cavities attached to the walls [24,25] through the enhancement in the transport of carbon dioxide towards these cavities that, otherwise, would only grow by diffusion. A very similar effect is probably behind the long time scales involved in limnic eruptions. In these phenomena, bubbly plumes form that keep entraining CO_2-saturated water from the bottom of the lake until it is almost depleted of this gas due to the global overturning flow that they induce in the lake [6]. Altogether, the chain of effects described in this Letter leads to the fast appearance of foam that has granted beer tapping its popularity.

We would like to thank Dr. Maylis Landeau for her useful comments on the potential applications of the present study. The authors are indebted to Professors Norman Riley, José Manuel Gordillo, Alejandro Sevilla, and Carlos Martínez-Bazán for their insightful comments. We acknowledge the support of the Spanish Ministry of Economy and Competitiveness through Grant No. DPI2011-28356-C03-02.

*javier.rodriguez@uc3m.es

[1] Y. Zhang and G. W. Kling, Annu. Rev. Earth Planet Sci. **34**, 293 (2006).
[2] Y. Zhang, Nature (London) **379**, 57 (1996).
[3] K. V. Cashman and R. S. J. Sparks, Geol. Soc. Am. Bull. **125**, 664 (2013).
[4] M. Mangan, L. Mastin, and T. Sisson, J. Volcanol. Geotherm. Res. **129**, 23 (2004).
[5] G. Liger-Belair, C. Cilindre, R. D. Gougeon, M. Lucio, I. Gebefügi, P. Jeandet, and P. Schmitt-Koppling, Proc. Natl. Acad. Sci. U.S.A. **106**, 16545 (2009).
[6] R. W. Mott and A. W. Woods, J. Volcanol. Geotherm. Res. **192**, 151 (2010).
[7] See Supplemental Material at http://link.aps.org/supplemental/10.1103/PhysRevLett.113.214501 for further

details of the experimental setup, high speed movies of the experiments and additional calculations.

[8] C. E. Brennen, *Cavitation and Bubble Dynamics* (Oxford University Press, Oxford, 1995).

[9] W. Goldsmith, *Impact: The Theory and Physical Behaviour of Colliding Solids* (Dover Publications, New York, 2001).

[10] S. B. Feinstein, F. J. Ten Cate, W. Zwehl, K. Ong, G. Maurer, C. Tei, P. M. Shah, S. Meerbaum, and E. Corday, J. Am. Coll. Cardiol. **3**, 14 (1984).

[11] M. P. Brenner, S. Hilgenfeldt, and D. Lohse, Rev. Mod. Phys. **74**, 425 (2002).

[12] C. E. Brennen, J. Fluid Mech. **472**, 153 (2002).

[13] A. Prosperetti and G. Seminara, Phys. Fluids **21**, 1465 (1978).

[14] G. Iooss, P. Laure, and M. Rossi, Phys. Fluids A **1**, 915 (1989).

[15] P. S. Epstein and M. S. Plesset, J. Chem. Phys. **18**, 1505 (1950).

[16] C. D. Ohl, O. Lindau, and W. Lauterborn, Phys. Rev. Lett. **80**, 393 (1998).

[17] J. S. Turner, Proc. R. Soc. A **239**, 61 (1957).

[18] B. R. Morton, J. Fluid Mech. **9**, 107 (1960).

[19] M. C. Rogers and S. W. Morris, Phys. Rev. Lett. **95**, 024505 (2005).

[20] N. Vladimirova, Combust. Theory Modell. **11**, 377 (2007).

[21] M. C. Rogers and S. W. Morris, Chaos **22**, 037110 (2012).

[22] T. S. Coffey, Am. J. Phys. **76**, 551 (2008).

[23] A. W. Woods, Annu. Rev. Fluid Mech. **42**, 391 (2010).

[24] S. F. Jones, G. M. Evans, and K. P. Galvin, Adv. Colloid Interface Sci. **80**, 27 (1999).

[25] G. Liger-Belair, C. Voisin, and P. Jeandet, J. Phys. Chem. B **109**, 14573 (2005).